Academic Journal of Applied Sciences
ISSN: 3105-0549 (Print), ISSN: 3105-0557 (Online) | Vol. 1, No. 1, 2026

3D Borehole to Surface Electromagnetic Inversion Based on Upscaling network

Qian Zhang

School of Physics and Electronic Information Engineering, Henan Polytechnic University, Jiaozuo, Henan 454000, China

Abstract: Borehole-to-surface electromagnetic method, due to its transmitter source being located in the borehole, can more directly excite electromagnetic responses from deep formations compared to surface electromagnetic methods, effectively improving the detection resolution of deep targets. However, for steel-cased wells, the casing possesses extremely high electrical conductivity, and the casing effect cannot be ignored in the data processing of borehole-to-surface electromagnetic surveys. Direct discrete modeling of slender hollow steel casings is both difficult and unfavorable for subsequent inversion calculations. Therefore, this paper proposes a three-dimensional borehole-to-surface electromagnetic inversion method based on an upscaling network. First, through unsupervised deep learning, the method establishes a nonlinear mapping between the electromagnetic response of fine-grid models containing casings and equivalent coarse-grid models, training an upscaling network from fine-scale grids to coarse-scale grid electrical structures. Second, the upscaled coarse-grid information is used as the initial model to perform three-dimensional borehole-to-surface electromagnetic inversion. Finally, the accuracy and feasibility of the proposed method are verified through three-dimensional borehole-to-surface electromagnetic inversion examples, and the inversion capability for deep targets is analyzed through synthetic data models, examining sensitivity regions, single-transmitter wells, and dual-transmitter wells.

Keywords: Borehole-to-surface electromagnetic; Upscaling; Deep residual network; Three-dimensional inversion.

1. Introduction

The borehole-to-surface electromagnetic method (Borehole-to-Surface Electromagnetic Method, BTS-EM) is an effective technique for investigating deep subsurface electrical structures [1–3]. Compared with conventional electromagnetic exploration methods, BTS-EM deploys transmitters within boreholes and measures electromagnetic fields at the surface, enabling a more direct excitation of deep formations. This approach effectively characterizes the three-dimensional resistivity distribution and fluid variations in hydrocarbon reservoirs, thereby improving the resolution of deep targets [4–6]. With recent advances in BTS-EM technology, this method has been increasingly applied in the exploration of conventional and unconventional hydrocarbons, as well as emerging energy resources [7–9].

At present, borehole-to-surface electromagnetic (BTS-EM) surveys are often conducted in steel-cased wells. Due to the extremely small thickness of the casing (on the order of millimeters), its kilometer-scale length, and its high electrical conductivity, pronounced multiscale characteristics arise [10–14]. These characteristics significantly affect the electromagnetic fields around the borehole and pose substantial challenges for inversion [15–16]. To address these challenges, various approaches have been proposed to mitigate the impact of multiscale effects in BTS-EM.

One approach is to explicitly model multiscale media and perform forward simulations. Um et al. [17] employed a tetrahedral finite-element method to model steel casings and fractures and conducted numerical simulations of transient electromagnetic responses in formations containing steel-cased wells. Commer et al. [18] used a structured hexahedral finite-difference method to compute current density distributions in fractured rock formations in the presence of casing and analyzed the detectability of deep targets. Even when adaptive mesh refinement techniques are employed, such as locally refined octree meshes [19] or adaptive tetrahedral meshes [20], these approaches typically require millions of degrees of freedom, leading to slow convergence of iterative solvers and a significantly increased computational burden.

Another approach is to replace multiscale media with equivalent models to achieve upscaling of steel-cased well models. Weiss [21] proposed a finite-element method based on hierarchical models, in which electrical conductivity is assigned to the edges and faces of mesh elements to represent small-scale features such as casings or fractures with varying conductivities. Schwarzbach and Haber [22] introduced a technique that combines homogenization with the inversion process, where cells surrounding the steel casing are merged into equivalent units, improving modeling accuracy while minimizing computational cost. Um et al. [23] approximated steel casings as a combination of long linear ideal conductors and short solid conductive prisms, significantly reducing the number of discretization elements required for modeling. This approach was further validated using logging data collected in Alberta, Canada, demonstrating its robustness in heterogeneous geological settings. However, these methods still exhibit limitations when dealing with complex geometries and often require additional computational resources for calculating the electromagnetic responses of equivalent models.

In recent years, machine learning methods have achieved rapid development in the field of upscaling due to their high efficiency and strong nonlinear mapping capabilities [24–27]. Wang et al. [28] trained a deep convolutional neural network (Convolutional Neural Network, CNN) to learn the relationship between coarse-grid and fine-grid models, thereby enabling the upscaling of fine-scale geological models. Wang et al. [29] further proposed a deep learning-based upscaling framework that bridges pore-scale and field-scale processes by modeling pore-scale mineral precipitation within meter-scale fracture systems and incorporating these effects into macroscopic simulations, achieving multiscale modeling across five orders of magnitude.

However, applications of upscaling methods for multiscale media in the electromagnetic domain remain relatively limited.

In this study, we propose a residual neural network-based upscaling strategy for steel-cased wells. The proposed method employs a residual network to learn the nonlinear relationship between fine-grid electromagnetic models and coarse-grid equivalent models, enabling upscaling through an unsupervised learning framework without requiring a large amount of labeled equivalent resistivity data. By computing the three-dimensional sensitivity of BTS-EM, the effective imaging region is analyzed. Furthermore, the obtained equivalent steel-cased well model is used as the initial model for three-dimensional borehole-to-surface electromagnetic inversion.

2. 3D Electromagnetic Inversion Method Based on Upscaling Network

This study proposes a two-stage three-dimensional borehole–surface electromagnetic inversion method based on a scale-up neural network.In the first stage, a deep neural network-based scale-up model is introduced. A residual network is employed to perform scale-up transformation on the fine-scale cased borehole electromagnetic model, thereby obtaining the equivalent electrical property distribution on a coarse-scale grid.In the second stage, the resulting scale-up model is used as the initial model for inversion. By incorporating borehole–surface electromagnetic response data, a three-dimensional regularized inversion algorithm is applied to iteratively solve for and image the subsurface resistivity structure.

2.1. Upscaling Method for Cased Wells

This paper constructs a scale-up method based on unsupervised learning using a residual neural network to establish the nonlinear mapping relationship between the electromagnetic responses of fine-grid cased-hole models and the equivalent resistivity parameters of coarse-grid models. We define a function as follows:

$$Y = f(X, G, d) \quad (1)$$

X represents the electromagnetic response calculated from the fine-grid model, G denotes the geometric parameters of the cased-hole model (such as outer diameter, inner diameter, depth, etc.),d is the background layer resistivity, Y is the equivalent body resistivity in the target coarse grid. The function f is typically highly nonlinear and difficult to obtain directly. Therefore, in the absence of true values for the equivalent parameters, an approximate solution for the coarse-grid parameters can be achieved by using a neural network combined with an unsupervised feedback mechanism based on response residuals。 The neural network approximates Y for different cased-hole models through the following mapping equation:

$$f_{\theta}: X, \quad , d \rightarrow Y \quad (2)$$

Where θ represents the parameters of the neural network (including weights and biases),, $d = [d_1, d_2, d_3, \ldots]$ denotes the background layer resistivity parameters., If the background layer resistivity vector remains unchanged during each computation, the mapping in Equation (2) can be simplified to:

$$f_{\theta}: X, \quad \rightarrow Y \quad (3)$$

Equation (3) indicates that, given a training set, training the neural network enables an approximate mapping of the resistivity parameters.

The workflow diagram of the scale-up method is shown in Figure 1. The scale-up method workflow mainly consists of the following three steps. First, dataset construction is performed by conducting three-dimensional electromagnetic forward modeling on fine-grid cased-hole models to generate the response dataset required for network training. Second, network model training is carried out by building a deep learning model based on a residual neural network, which establishes the nonlinear mapping relationship between the fine-grid electromagnetic responses and the equivalent coarse-grid models, followed by training of the network. Third, scale-up of the cased-hole model is achieved by inputting the response data from a real cased-hole model into the trained network, thereby obtaining the upscaled coarse-grid electrical structure (resistivity distribution). In summary, this process enables efficient approximation of equivalent coarse-grid resistivity parameters from fine-grid electromagnetic responses through an unsupervised or residual-guided neural network approach.

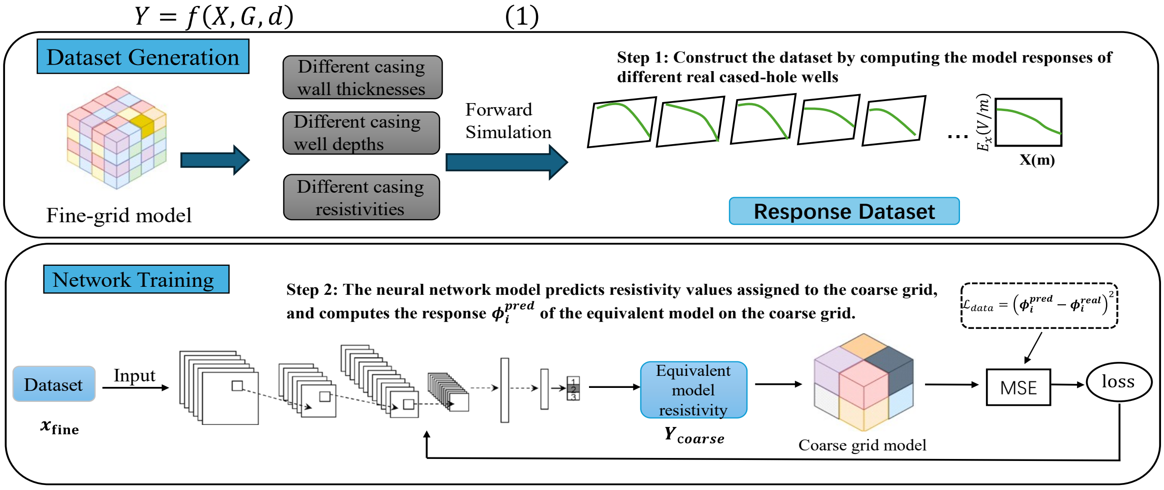

Figure 1. Upscaling Method for Cased Wells

2.2. Dataset construction

The model schematic is shown in Figure 2. The cased borehole geometric parameters (including outer diameter, inner diameter, depth, etc.) and electrical parameters such as formation background resistivity, borehole fluid resistivity, and casing resistivity are used as variables to generate the cased borehole model.

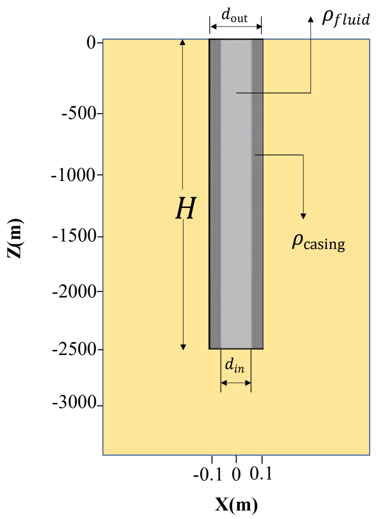

Figure 2. Schematic Diagram of the Cased Borehole Model

The borehole depth (H) of the cased borehole model is set to vary within the range of 500–4000 m, the inner diameter (d_in) ranges from 0.05–0.15 m, and the outer diameter (d_out) ranges from 0.10–0.25 m, subject to the physical constraint d_out > d_in to ensure a reasonable casing wall thickness. The model is placed in a half-space environment, with background resistivity (ρ_bg) ranging from 1–10000 Ω·m, borehole fluid resistivity (ρ_fluid) ranging from 0.01–10 Ω·m, and casing resistivity (ρ_casing) set between 1×10^{-6} and 1×10^{-4} Ω·m. The parameter ranges are summarized in Table 1.

The transmitter source is placed inside the borehole, and the receiver array consists of a dense electric field receiver array distributed within a 2 km radius around the borehole. Response data for different models are obtained through three-dimensional forward modeling computations. Effective data preprocessing reduces the difficulty of network training. To eliminate magnitude differences arising from different parameter combinations, logarithmic transformation and normalization are applied to all response values, resulting in a smoother data distribution and avoiding excessively large or small gradients during training. A total of 8000 samples are simulated in this study, with 80% used for training and 20% for testing, ultimately generating a dataset suitable for the model.

Table 1. Parameter Range Table

Model Parameter	Range
Borehole Depth	[500,4000]
Background Resistivity	[1,10000]
Casing Resistivity	[1e-6,1e-4]
Fluid Resistivity	[0.01,10]
Inner Diameter	[0.05,0.15]
Outer Diameter	[0.10,0.25]

2.3. Network Training

This study employs a residual network model based on the PyTorch framework for training. For the constructed dataset, the forward response data input for each cased borehole model has a matrix dimension of 22 (number of receivers) × 1 (total number of transmitters) × 2 (electric field component values). Feature extraction is first performed through an initial fully connected layer combined with a normalization layer and ReLU activation function, followed by a feature projection layer for dimensionality reduction. The backbone network consists of 3 residual blocks, each comprising two fully connected layers, a batch normalization layer, a ReLU activation function, and a Dropout layer, with residual learning achieved through skip connections. Finally, an output branch is connected, which outputs the conductivity parameters through two fully connected layers and a Sigmoid activation function. Based on the sample data, the optimal hyperparameter settings are determined as follows: batch size of 200, learning rate of 1×10^{-4}, number of training epochs of 400, and Dropout rate of 0.2. ReLU is used as the activation function throughout the network, and the model is trained using the Adam optimizer, which serves as a more robust alternative to stochastic gradient descent.

The learning rate, as a critical hyperparameter controlling the step size of parameter optimization, directly affects the convergence behavior and final performance of the model. This study adopts a dynamic learning rate adjustment strategy based on exponential decay, which takes the form:

$$lr_t = lr_0 \times \gamma^t \tag{4}$$

Where lr_t denotes the learning rate at epoch t, lr_0 is the initial learning rate, and the learning rate decay factor $\gamma = 0.9$. This strategy achieves continuous exponential decay of the learning rate: after each training epoch, the learning rate is reduced by a factor of 0.9, which ensures rapid convergence in the early stages while maintaining stability in the later stages, thereby improving overall training performance.

In the traditional supervised learning framework, the evaluation of model performance typically relies on accuracy metrics in the parameter space. Commonly used metrics include Mean Square Error (MSE) and Mean Squared Log Error (MSLE). However, in the cased borehole scale upgrading problem studied in this paper, the true parameter values of the coarse grid equivalent model are unknown, and training the network model using conventional loss functions cannot guarantee the reasonableness of the results. Therefore, we shift the optimization objective from the parameter space to the observable response space, and adopt a physics-constrained self-supervised mechanism during training. For each set of equivalent model resistivities predicted by the network, a tensor grid is used to compute the forward electromagnetic response d_{pred} of the model and compare it with the fine model response d_{fine}, and the residual between them is used to construct the loss function.

$$\text{Loss} = \frac{1}{N_d}\sum_{j=1}^{N_d}\left[\lg\left(\left|d_{fine}^{(j)}\right|\right) - \lg\left(\left|d_{pred}^{(j)}\right|\right)\right]^2 \tag{5}$$

Where N_d denotes the number of observed data points, $d_{fine}^{(j)}$ represents the forward response of the fine model at the j-th measurement point, and, $d_{pred}^{(j)}$ represents the forward response computed by the predicted model.

3. Numerical Simulation Analysis

3.1. Cased Borehole Upscaling Validation

For 100 newly generated upscaling models, the histogram in Figure 3 shows the distribution of R^2 values (coefficients of determination) between the predicted values and the numerical solutions of the input models. The results indicate that the R^2 values of most samples are distributed in the high-value interval above 0.85, validating the accuracy of the upscaling network in upscaling fine-grid models under different combinations of model parameters. The response residual loss function measures whether the coarse model can accurately fit the fine model at the level of electromagnetic response; by minimizing the residual between the electromagnetic responses of the fine model and the coarse model, backpropagation is used to update the parameters and guide the neural network in learning the inter-scale mapping relationship. A smaller mean absolute error of the response indicates a better fit between the equivalent model after upscaling and the true model. The training loss and validation loss curves are shown in Figure 4, both exhibiting a clear downward trend as the number of training iterations increases, indicating that the model is progressively learning the features of the data. After approximately 200 iterations, the curves stabilize without overfitting. The validation loss decreases rapidly in the early stage and then levels off. The training results demonstrate the reasonableness of the network training approach proposed in this study.

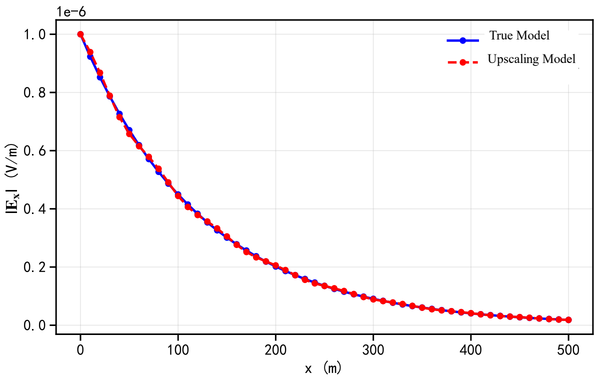

Figure 3. Histogram of R^2 values

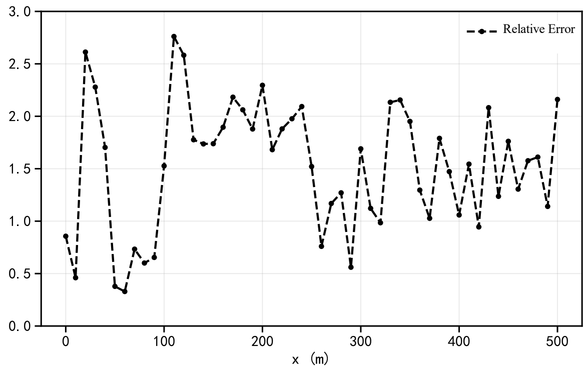

Figure 4. Training Loss

3.2. Borehole-to-Surface Electromagnetic Sensitivity Analysis

To investigate the sensitivity characteristics of BTS-EM inversion imaging, we compute its three-dimensional sensitivity distribution and analyze the effective imaging region of BTS-EM. Figure 5 presents the normalized sensitivity distribution (in base-10 logarithm) of the background model at a frequency of 20 Hz. The vertical electric dipole source is located directly below the cased borehole, with a formation resistivity of 8 Ω·m. The receivers are located at: (a) (300, 0, 0) m, (b) (600, 0, 0) m, and (c) (1000, 0, 0) m. The high-sensitivity region forms an inclined arc defined by the transmitter-receiver pair. By deploying a surface receiver array ($x > 0$ m, $y = 0$ m), BTS-EM can detect an inverted right-triangle region bounded by the transmitter, the receiver array, and the casing location. When the surface receivers are arranged in a grid pattern, BTS-EM can illuminate a cone-like subsurface volume. This sensitivity distribution indicates that BTS-EM is particularly well-suited for monitoring the upward migration of fluids or gases.

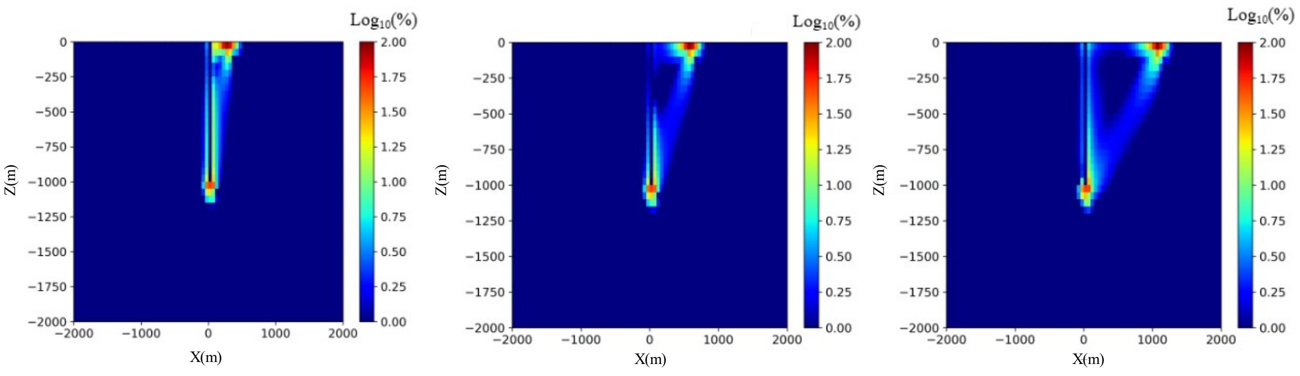

(a) (b) (c)

Figure 5. Sensitivity Distribution

3.3. Inversion Case Analysis of Low-Resistivity Anomalous models

The upscaling method is applied to BTS-EM modeling and imaging of low-resistivity target bodies, with inversion experiments conducted using a densely distributed surface receiver array. The receivers cover an area of 3 km × 3 km with a spacing of 100 m. The vertical well extends from (0, 0, 0) m to (0, 0, −1500) m. The inversion domain is constrained between −1500 m and 0 m, with background resistivity and target resistivity set to 100 Ω·m and 2 Ω·m, respectively. A three-dimensional geoelectric model of a low-resistivity dipping reservoir is constructed, with a horizontal extent of 200 m in the x-direction and a burial depth ranging from −600 m to −1000 m below the surface. The model schematic is shown in Figure 6.

The initial model is a homogeneous half-space model with a background resistivity of 100 Ω·m. The transmitter frequency range spans from 1 Hz to 1000 Hz, with 11 logarithmically spaced frequency points selected. Gaussian random noise of 1% was added to the data. A total of 16 iterations were performed during the inversion process, with the data misfit decreasing from an initial value of 7.53 to 0.832. The inversion results are visualized in Figure 7, which presents the xy, xz, and yz cross-sectional views. Although the recovered target is slightly thicker than the true target, BTS-EM reasonably reconstructs the overall geometry and resistivity distribution of the target body.

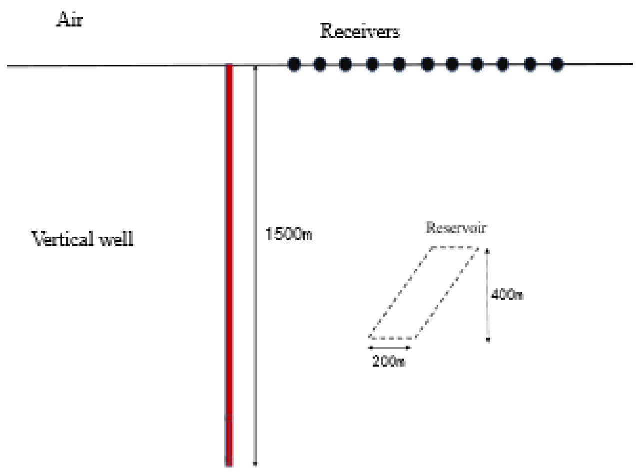

Figure 6. Schematic Diagram of the True Model

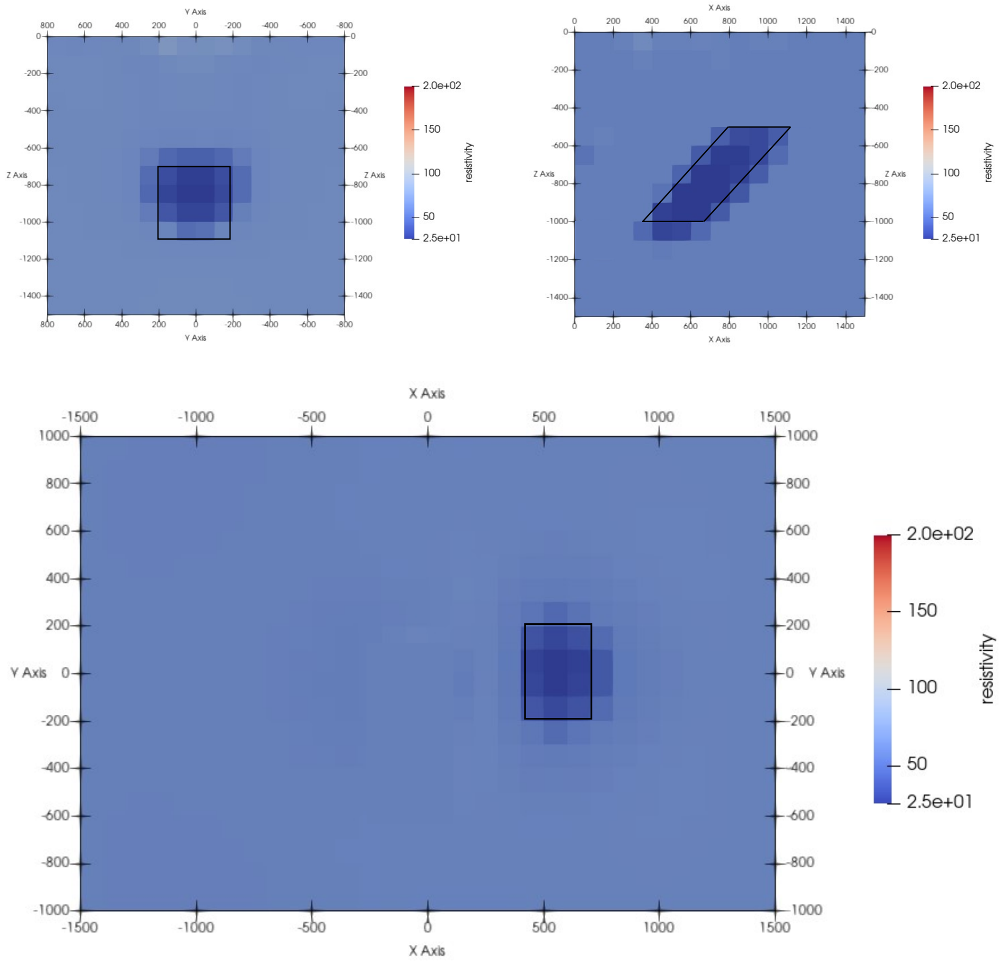

Figure 7. Three-Dimensional Inversion Result

4. Conclusion

This study introduces a scale-up-based borehole-to-surface electromagnetic inversion method to overcome the difficulties of multi-scale modeling and inversion under steel-cased well conditions. By employing deep learning, a nonlinear mapping is established from fine-scale electromagnetic responses to equivalent coarse-scale models. Utilizing the upscaled coarse-grid model as the starting model for 3D inversion yields resistivity distributions with sharper boundaries and improved imaging precision, validating the effectiveness and practicality of the proposed scale-up approach in borehole-to-surface electromagnetic inversion.

References

[1] Cao Hui, Mao Lifeng, Wang Xuben, et al. Physical simulation experiment on borehole-to-surface electromagnetic responses[J]. Oil Geophysical Prospecting, 2013, 48(6): 995-998.

[2] .Li Tingting, Wang Jia, Zhu Kaiguang. Research on the exploration depth of the borehole-surface electromagnetic field[J]. Progress in Geophysics, 2013, 28(1): 373-379.

[3] Tsourlos P, Ogilvy R, Papazachos C, et al. Measurement and inversion schemes for single borehole-to-surface electrical resistivity tomography surveys[J]. Journal of Geophysics and Engineering, 2011, 8(4): 487.
[4] .QIN Ce, FU Wenliang, WANG Xuben, et al.Three-dimensional anisotropic forward modeling algorithm for borehole-to-surface electromagnetic method using non-conforming meshes and high-order finite element[J]. Oil Geophysical Prospecting, 2024, 59(6): 1410-1419.
[5] Colombo D, McNeice G W. Quantifying surface-to-reservoir electromagnetics for waterflood monitoring in a Saudi Arabian carbonate reservoir[J]. Geophysics, 2013, 78(6): E281-E297.
[6] Bai Z, Tan M J, Zhang F L. Three-dimensional forward modeling and inversion of borehole-to-surface electrical imaging with different power sources[J]. Applied Geophysics, 2016, 13(3): 437-448.
[7] Cao Hui, Wang Xuben, He Zhanxiang, et al. Calculation of borehole-to-surface electromagnetic responses on horizontal stratified earth medium[J]. Oil Geophysical Prospecting, 2012, 47(2): 338-343.
[8] Colombo D, McNeice G, Cuevas N, et al. "Surface to borehole electromagnetics for 3D waterflood monitoring: Results from first field deployment." SPE Annual Technical Conference and Exhibition?. SPE, 2018.
[9] Hoversten G M, Schwarzbach C, Belliveau P, et al. "Borehole to surface electromagnetic monitoring of hydraulic fractures." 79th EAGE Conference and Exhibition 2017. Vol. 2017. No. 1. European Association of Geoscientists & Engineers, 2017.
[10] Streich R. Controlled-source electromagnetic approaches for hydrocarbon exploration and monitoring on land[J]. Surveys in geophysics, 2016, 37(1): 47-80.
[11] Puzyrev V, Vilamajo E, Queralt P, et al. Three-dimensional modeling of the casing effect in onshore controlled-source electromagnetic surveys[J]. Surveys in Geophysics, 2017, 38: 527-545.
[12] Patzer C, Tietze K, Ritter O. Steel-cased wells in 3-D controlled source EM modelling[J]. Geophysical Journal International, 2017, 209(2): 813-826.
[13] Heagy L J, Oldenburg D W. Modeling electromagnetics on cylindrical meshes with applications to steel-cased wells[J]. Computers & Geosciences, 2019, 125: 115-130.
[14] Cuevas N H. Insights on electromagnetic scattering by steel casings in surface-to-borehole and borehole-to-surface methods[J]. The Leading Edge, 2022, 41(2): 93-99.
[15] Marsala A F, Al-Buali M, Ali Z, et al. "First pilot of borehole to surface electromagnetic in saudi arabia-a new technology to enhance reservoir mapping & monitoring." 73rd EAGE Conference and Exhibition incorporating SPE EUROPEC 2011. European Association of Geoscientists & Engineers, 2011.
[16] Tietze K, Patzer C, Ritter O, et al. "3D inversion of controlled-source electromagnetic data in the presence of steel-cased wells." 78th EAGE Conference and Exhibition 2016. Vol. 2016. No. 1. European Association of Geoscientists & Engineers, 2016.
[17] Um E S, Commer M, Newman G A, et al. Finite element modelling of transient electromagnetic fields near steel-cased wells[J]. Geophysical Journal International, 2015, 202(2): 901-913.
[18] Commer M, Hoversten G M, Um E S. Transient-electromagnetic finite-difference time-domain earth modeling over steel infrastructure[J]. Geophysics, 2015, 80(2): E147-E162.
[19] Qin C, Li H, Li H, et al. High-order finite-element forward-modeling algorithm for the 3D borehole-to-surface electromagnetic method using octree meshes[J]. Geophysics, 2024, 89(4): F61-F75.
[20] Castillo-Reyes O, Modesto D, Queralt P, et al. 3D magnetotelluric modeling using high-order tetrahedral Nédélec elements on massively parallel computing platforms[J]. Computers & Geosciences, 2022, 160: 105030.
[21] Weiss C J. Finite-element analysis for model parameters distributed on a hierarchy of geometric simplices[J]. Geophysics, 2017, 82(4): E155-E167.
[22] Schwarzbach, Christoph, and Eldad Haber. "Improved upscaling of steel-cased wells through inversion." SEG International Exposition and Annual Meeting. SEG, 2018.
[23] Um E S, Kim J, Wilt M. 3D borehole-to-surface and surface electromagnetic modeling and inversion in the presence of steel infrastructure[J]. Geophysics, 2020, 85(5): E139-E152.
[24] Liu B, Guo Q, Li S, et al. Deep learning inversion of electrical resistivity data[J]. IEEE Transactions on Geoscience and Remote Sensing, 2020, 58(8): 5715-5728.
[25] Puzyrev V. Deep learning electromagnetic inversion with convolutional neural networks[J]. Geophysical Journal International, 2019, 218(2): 817-832.
[26] Liao Q, Lei G, Zhang D, et al. Analytical solution for upscaling hydraulic conductivity in anisotropic heterogeneous formations[J]. Advances in Water Resources, 2019, 128: 97-116.
[27] Li H, Durlofsky L J. Ensemble level upscaling for compositional flow simulation[J]. Computational Geosciences, 2016, 20(3): 525-540.
[28] Wang N, Liao Q, Chang H, et al. Deep-learning-based upscaling method for geologic models via theory-guided convolutional neural network[J]. Computational Geosciences, 2023, 27(6): 913-938.
[29] Wang Z, Battiato I. A deep learning upscaling framework: Reactive transport and mineral precipitation in fracture-matrix systems[J]. Advances in Water Resources, 2024, 183: 104588.